Vol. 689: 33–46, 2022
https://doi.org/10.3354/meps14032

MARINE ECOLOGY PROGRESS SERIES
Mar Ecol Prog Ser

Published May 12

Gulf ribbed mussels increase plant growth, primary production, and soil nitrogen cycling potential in salt marshes

Ryann E. Rossi[1,3,*], Charles A. Schutte[1,4], Jordan Logarbo[1,2], Caleb Bourgeois[1], Brian J. Roberts[1]

[1]Louisiana Universities Marine Consortium (LUMCON), Chauvin, LA 70344, USA
[2]School of Renewable Natural Resources, Louisiana State University Agricultural Center, Baton Rouge, LA 70803, USA

[3]*Present address:* Oak Ridge Institute for Science and Education, US Environmental Protection Agency, Gulf Breeze, FL 32561, USA
[4]*Present address:* Department of Environmental Science, Rowan University, Glassboro, NJ 08028, USA

ABSTRACT: Smooth cordgrass *Spartina alterniflora* and Atlantic ribbed mussels *Geukensia demissa* have a mutualism whereby *S. alterniflora* provides substrate and shade for *G. demissa* while *G. demissa* enhances *S. alterniflora* growth and drought tolerance. Together, these species improve salt marsh stability and function. To better understand if a similar relationship exists between *S. alterniflora* and Gulf ribbed mussels *G. granosissima* in salt marshes of the Gulf of Mexico, we conducted a manipulative experiment with identical starting plant density and varying densities of *G. granosissima* and monitored plant and soil responses over a growing season. We found that *S. alterniflora* stem and leaf density was 1.5 and 1.9 times greater for the highest mussel biomass compared to the lowest mussel biomass treatments. Similarly, above- and below-ground biomass were 2.6 and 3.2 times greater for the highest mussel biomass compared to the lowest mussel biomass treatments. More and larger *S. alterniflora* at higher *G. granosissima* densities resulted in 2 and 4 times the *S. alterniflora* gross CO_2 uptake and respiration rate, respectively. Methane fluxes were highest when *G. granosissima* were present, likely driven by the positive relationship between methane flux and belowground biomass. Net potential nitrification was 5 times higher for the highest mussel biomass compared to the lowest mussel biomass treatments, and denitrification rates were 1.8 times higher. Ultimately, our results suggest that *G. granosissima* increases *S. alterniflora* growth and productivity, much like the positive relationship between *G. demissa* and *S. alterniflora*, which in turn influences salt marsh stability and function.

KEY WORDS: Ribbed mussel · Salt marsh · *Spartina alterniflora* · *Geukensia granosissima* · Nitrogen cycle · Greenhouse gas fluxes

1. INTRODUCTION

Salt marshes exist in dynamic coastal environments characterized by frequent fluctuations in inundation, temperature, salinity, and nutrient availability. The organisms that inhabit these ecosystems must adapt to tolerate the stressful conditions. Facilitative interactions are important mechanisms in maintaining ecosystem function and stability and are particularly important in salt marshes because they can reduce physical stress (Stachowicz 2001, Bruno et al. 2003). These interactions may impact how salt marshes pro-

*Corresponding author: ryann.rossi@gmail.com

vide ecosystem services such as carbon sequestration, flood mitigation, and nitrogen removal (Culhane et al. 2018).

Atlantic ribbed mussels *Geukensia demissa* (Dillwyn, 1817) are found throughout Atlantic salt marshes and are associated with smooth cordgrass *Spartina alterniflora* Loisel (Bertness 1984). *G. demissa* can tolerate variations in salinity and are more common in *S. alterniflora*-dominated marshes with salinities of 18–30 (Bertness 1984, Chintala et al. 2006). Nutrient rich biodeposits from *G. demissa* pseudofeces increase nutrient availability in porewater and soil, which can increase *S. alterniflora* growth and vegetative expansion (Jordan & Valiela 1982, Bertness 1984, Angelini et al. 2016, Derksen-Hooijberg et al. 2018). *G. demissa* also reduce porewater salinity and increase water storage via pseudofeces and by the creation of pore spaces by themselves and the crabs (and the crab burrows) that they facilitate (Angelini et al. 2015, 2016). *G. demissa* may further promote *S. alterniflora* growth and survival by reducing sulfide stress, either by increasing porewater iron (via iron-rich pseudofeces), which can bind and precipitate sulfide, or by sulfide oxidation in mussel gill mitochondria (Derksen-Hooijberg et al. 2018). In turn, *S. alterniflora* provides substrate for *G. demissa* byssal thread attachment, prevents *G. demissa* desiccation via shading, and provides a potential food source (Bertness 1984, Bertness & Leonard 1997, Kreeger & Newell 2001). This mutualism also influences nitrogen cycling processes, such as denitrification and nitrification, which increase in the presence of both *S. alterniflora* and *G. demissa*, suggesting that this positive relationship may influence salt marsh nitrogen cycling and nitrogen removal (Bilkovic et al. 2017, Zhu et al. 2019). *G. demissa* also enhance water quality by removing nutrients and fecal bacteria (Durand et al. 2020, Moody & Kreeger 2020).

In the Gulf of Mexico (GoM), a different ribbed mussel species, the Gulf ribbed mussel *G. granosissima* (G. B. Sowerby III, 1914), inhabits salt marshes. *G. granosissima* is often associated with both *Juncus roemarianus* (Scheele) and *S. alterniflora* and tends to be more common at sites with mean salinities over 3.5 and on the marsh edge (Honig et al. 2015, Logarbo 2021). These slight differences in *G. granosissima* ecology, compared to *G. demissa*, may or may not influence the relationship between *G. granosissima* and dominant marsh plant species. More work is needed to explore the relationship between *G. granosissima* and *S. alterniflora* in the GoM to determine if the relationship is similar to *G. demissa* and *S. alterniflora* in Atlantic marshes. Here, we report on a field experiment with manipulated *G. granosissima* densities over a summer to early autumn growing season in which we hypothesize that *S. alterniflora* and *G granosissima* in GoM marshes will have a similar positive relationship to the one shared by *S. alterniflora* and *G. demissa* in Atlantic coast marshes. We expect that as *G. granosissima* density increases so would *S. alterniflora* productivity and biomass, and soil nitrogen-cycling process rates, much like the positive relationship found between *G. demissa* and *S. alterniflora*. We manipulated *G. granosissima* density by co-transplanting *G. granosissima* with *S. alterniflora* in 5 mussel addition treatments (n = 4 replicates) that capture the range in *G. granosissima* densities recorded throughout *S. alterniflora*-dominated marshes in Louisiana (Honig et al. 2015, Logarbo 2021). We measured aboveground plant metrics and productivity weekly throughout the growing season, and measured greenhouse gas fluxes, soil nitrogen-cycling process rates, soil nitrogen content, and *G. granosissima* and total *S. alterniflora* biomass at the end of the experiment.

2. MATERIALS AND METHODS

2.1. Study site description

The experiment was deployed in a *Spartina alterniflora*-dominated salt marsh in Cocodrie, LA, near the DeFelice Marine Center of the Louisiana Universities Marine Consortium (LUMCON) (29.2561° N, 90.6669° W) from June to October 2018. Marshes near LUMCON experience low tidal range (~0.3 m), mainly driven by wind (Hill & Roberts 2017). Other plant species present include *Juncus roemarianus*, *Distichlis spicata*, and *S. patens* (Hill & Roberts 2017). The mean (±SD) daily air temperature was 27.1 ± 2.6°C (range 18–29°C), mean daily wind speed was 3.7 ± 1.3 m s^{-1} (range 1–8 m s^{-1}), and daily mean precipitation was 0.01 ± 0.02 mm (range 0–0.14 mm). The mean daily salinity during the study period was 8.8 ± 3.9 (range 2–17), and mean daily water temperature was 29.5 ± 2.2°C (range 20–32°C). All daily measures were recorded at the LUMCON Marine Center environmental monitoring station (http://weatherstations.lumcon.edu/index.html) located ~380 m from the experiment.

Throughout this region, *Geukensia granosissima* densities vary. Mean excavated mussel densities for

Barataria and Hackberry Bays, LA, were 82 ± 18 and 66.6 ± 16.3 ind. m^{-2}, respectively (Spicer 2007, Honig et al. 2015). Surface densities of *G. granosissima* up to 350 m^{-2} have been documented in Sister Lake, LA (Logarbo 2021), with excavated densities between 754 and 8704 ind. m^{-2} (A. McDonald et al. pers. obs.). To our knowledge, no data are available on average aggregation size of *G. granosissima*.

2.2. Experimental design and setup

PVC tubes (10 cm diameter, n = 20) were used as experimental units which were oriented vertically. Each experimental unit was 72 cm long and had 50 holes (4.7 mm diameter) drilled randomly along the tube to allow lateral and vertical pore water movement. All experimental units were filled with homogenized marsh pond sediment that was sieved to remove roots and organisms and capped at the bottom. *G. granosissima* and *S. alterniflora* were co-transplanted into each experimental unit with 4 replicate units for each of the 5 treatments (Fig. S1 in Supplement 1 at www.int-res.com/articles/suppl/m689p033_supp1.pdf). We only used *S. alterniflora*, as this is the dominant marsh plant and is consistent with many studies involving *G. demissa*. *S. alterniflora* and *G. granosissima* specimens were collected in June 2018 from a marsh, approximately 100 m from experiment deployment, where both species were previously recorded. *G. granosissima* were separated from hooked mussels *Ischadium recurvum* in the field, and returned to the lab where they were cleaned of sediment and plant debris, and measured to the nearest mm. Only *G. granosissima* in the size range of 30–70 mm were used in the experiment, and the mean shell length of transplanted individuals was 55.5 ± 14.5 mm. *G. granosissima* were transplanted into tubes in the following initial densities: 0, 1, 2, 4, and 8 which corresponds to 0, 127, 254, 509, and 1018 mussels m^{-2}. We refer to the initial transplant densities (0, 1, 2, 4, and 8) as the treatments throughout the manuscript. These densities were chosen to capture the range in *G. granosissima* densities recorded throughout *S. alterniflora*-dominated Louisiana marshes. Specifically, we were interested in capturing densities closer to some of the higher densities observed (A. McDonald et al. pers. obs.). We selected *S. alterniflora* shoots that were 23.5 ± 3.6 cm tall to avoid older, taller plants and new shoots. We planted 3 *S. alterniflora* shoots in each tube, equivalent to approximately 382 stems m^{-2}, which aligns with reported mean densities in marshes adjacent to LUMCON (Hill & Roberts 2017).

Experimental units were deployed in a ~15 m diameter pond adjacent to a well-studied *S. alterniflora*-dominated salt marsh (Hill & Roberts 2017, Vastano et al. 2017, Bernhard et al. 2021). The pond was located at the head of a marsh creek ~35 m from its confluence with a larger estuarine channel. The site was chosen for its small size and isolation to reduce exposure to wind and boat-driven wave energy; the pond was protected on 3 sides by salt marsh, and was accessible only by kayak via a ~4 m channel. Experimental units were arranged in a square wooden frame following a marsh organ design (Morris 2007), but with each experimental unit positioned at the same level to generate uniform patterns of inundation and exposure (Fig. S1). The soil surface of the experimental units was level to the adjacent marsh platform to ensure natural tidal exposure. The marsh organ framework was placed on the north side of the pond 2 m from the shoreline to prevent shading from adjacent salt marsh plants.

2.3. Non-destructive sampling

Stem heights, stem density, and leaf density were measured weekly between June and October 2018 (n = 17). Treatments were maintained with replacement throughout the experiment to ensure treatment *G. granosissima* densities, but *G. granosissima* that recruited were not removed from any of the experimental units except for treatment 0. Density of other invertebrates (e.g. snail species) was also estimated weekly between June and October 2018.

At the end of the experiment (October 2018), all experimental units were transported intact to LUMCON for final destructive sampling. Experimental units were placed in large plastic containers filled with estuarine water collected at the study site to simulate *in situ* conditions. The water level in these containers was 1–2 cm below the soil surface in the experimental units. Experimental units were maintained in this way for less than 36 h between collection and destructive sampling to allow time for non-destructive measurements and sample processing. Stem heights, stem density, and leaf density were measured followed by gas flux measurements and then destructive sampling for *G. granosissima* biomass, plant above- and belowground biomass, soil properties, and nitrogen cycling process rate measurements.

2.4. Gas flux measurements and photosynthetic yield

Both light and dark CO_2 and CH_4 fluxes were measured using a Los Gatos Research ultraportable greenhouse gas analyzer (UGGA). Light and dark flux chambers were installed on each experimental unit, and the UGGA was connected to each flux chamber through ports in the chamber lid using gas-impermeable tubing. The total system volume was approximately 6.4 l. Gas was circulated within the flux chambers during flux measurements using small, battery-powered fans. The UGGA was connected to each chamber for 195 s with gas concentrations measured at 1 s frequency. Gas fluxes were calculated as the slope of the linear relationship between gas concentration and time. Only slopes with r^2 values >0.95 were used in subsequent analyses. Air temperature and irradiance were measured inside and outside the flux chambers at 15 s frequency using Hobo® pendant loggers (Onset). Gross CO_2 uptake, a proxy for photosynthesis, was calculated as the light chamber CO_2 flux (photosynthesis + respiration) minus the dark chamber CO_2 flux (respiration only).

Initial analyses comparing gross CO_2 uptake across different mussel treatments were confounded by the fact that gas flux measurements were made on a somewhat cloudy day with variable photosynthetically active radiation (PAR). This resulted in light-driven variability in measured light chamber CO_2 fluxes. We accounted for this variability in PAR by calculating the maximum gross CO_2 uptake. This value was derived by multiplying the measured maximum electron transport rate (ETR_{max}; described in detail below) by the measured gross CO_2 uptake divided by ETR_{max} at the light level at which each individual flux measurement was made (ETR_{light}):

$$\text{Max Gross } CO_2 = ETR_{max} \times \frac{\text{Gross}CO_2}{ETR_{light}} \quad (1)$$

Photosynthetic yield was measured using pulse amplitude modulation (PAM) fluorometry (Mini-PAM II, Walz) via rapid light curves (RLCs) which measures effective quantum yields over a range of increasing actinic light (Ralph & Gademann 2005). Measurements were taken on the third leaf from the top of the plant on a single live, green leaf from each experimental unit between 08:00 and 12:00 h using a leaf-clip holder and following the manufacturer-recommended protocol. RLCs were evaluated using WinControl-3 software, and photosynthetic efficiency and capacity were determined. Photosynthetic efficiency (alpha, α) is the initial slope of the RLC, and photosynthetic capacity (ETR_{max}) was calculated by fitting a hyperbolic tangent model equation and is measured in µmol electrons m^{-2} s^{-1} (Jassby & Platt 1976, Platt et al. 1980).

2.5. Destructive sampling

All aboveground plant tissue was clipped at the soil surface, dried, and weighed to a constant mass for biomass. Experimental units were extruded and sectioned into 0–10 and 10–30 cm intervals to quantify belowground biomass in addition to soil subsampling for soil properties, extractable nutrients, and potential nitrogen cycling rates (denitrification and nitrification). To quantify belowground biomass, sections were rinsed in deionized water, sieved, and separated into live and dead roots and rhizomes, then dried to a constant mass (Hill & Roberts 2017). *G. granosissima* were removed from each experimental unit, counted, and measured, and tissue was dried to a constant weight at ~80°C, then combusted to obtain ash-free dry mass to determine final *G. granosissima* biomass. Initial biomass (g m^{-2}) was estimated using an allometric equation (biomass = $a \times \text{length}^b$, where $a = 0.0000075$ and $b = 2.75$) based on the final *G. granosissima* biomass and lengths from the experiment (Fig. S2 in Supplement 1).

2.6. Soil physical and chemical properties

Approximately 5 g of fresh, homogenized soil were placed into an aluminum weigh boat, dried to a constant weight at ~80°C, and reweighed to calculate soil water content for each experimental unit. To measure extractable dissolved inorganic nitrogen, 2–3 g of soil were added to a 50 ml centrifuge tube along with 30 ml of 2 N KCl and then shaken at 250 rpm for 2 h. Samples were then centrifuged (2012 × *g*, 10 min), and the supernatant collected, filtered through a 0.2 µm filter, and stored frozen until analysis. Extractable NO_x (nitrate + nitrite) samples were measured using Cu–Cd reduction followed by azo colorimetry on a Lachat Instruments QuickChem® FIA+ 8000 Series Automated Ion Analyzer with an ASX-400 Series XYZ Autosampler as detailed by Marton & Roberts (2014). To prevent contamination of extractable NH_4-N samples by fumes from the NH_4Cl buffer used in NO_x analysis, NH_4-N was analyzed separately using phenate colorimetry (Greenberg et al. 1992). Standard curves were prepared by diluting NO_3-N and NH_4-N stock solutions (Hach) and yielded r^2 values of ≥ 0.99.

2.7. Potential nitrification rates

Potential nitrification rates were measured as described previously by Marton et al. (2015). Briefly, the incubation medium was prepared by diluting filtered seawater with deionized water to match the salinity measured in the field on the last day of the experiment. NH_4Cl and a 1:1 mix of K_2HPO_4 and KH_2PO_4 were added to final concentrations of 300 µmol l^{-1} N and 60 µmol l^{-1} P. A 2–3 g subsample of homogenized soil was placed into 50 ml centrifuge tubes (n = 4) and mixed thoroughly with 30 ml of the incubation medium. Tubes were incubated in the dark at 21°C and shaken gently at 325 rpm. One tube from each set of 4 was sacrificed at approximately 0.5, 12, 24, and 36 h to create a time series. Following incubation, each sample was centrifuged (3577 × *g*, 5 min), filtered through 0.20 µm syringe filters (Corning, #431224), and stored frozen until analysis for NO_x-N concentration as described in Section 2.6. Potential nitrification rates were calculated as the linear slope of NO_x-N concentration versus time and were corrected for incubation water volumes and soil dry weight. Potential rates are expressed in units of nmol N gDW^{-1} d^{-1} (where gDW is grams dry weight) throughout this manuscript.

2.8. Potential denitrification rates

Potential denitrification rates were measured using the acetylene inhibition technique (Sørensen 1978, Schutte et al. 2020). The incubation medium was prepared by diluting filtered seawater with deionized water to match the salinity measured in the field on the last day of the experiment. D-glucose ($C_6H_{12}O_6$), potassium nitrate (KNO_3), and potassium phosphate (KH_2PO_4) were added to the medium to final concentrations of 15 mmol C l^{-1}, 2000 µmol N l^{-1}, and 200 µmol P l^{-1}. A 15 g subsample of homogenized soil was weighed into a 125 ml flask and mixed thoroughly with 15 ml of the incubation medium. Flasks were sealed with rubber Suba-Seals. The flask headspace was then flushed with ultra-high purity nitrogen, and 10 ml of rinsed acetylene (C_2H_2) were added to the headspace. Flasks were incubated in the dark at 21°C and shaken gently at 250 rpm. Gas samples were collected from the flask headspace at 0.5, 1, 2, and 4 h to create a time series. At each time point, 10 ml of headspace gas were collected into a syringe and injected into a 5.9 ml Exetainer (Labco) that had been pre-purged with nitrogen. Immediately following sample collection, 9 ml of nitrogen and 1 ml of C_2H_2 were injected into the flask to maintain constant headspace composition and pressure throughout the incubation. Nitrous oxide (N_2O) concentrations were measured using a Shimadzu GC-2014 equipped with an electron capture detector. Potential denitrification rates were calculated as the linear slope of N_2O-N concentration versus time. Potential rates were corrected for incubation headspace volumes and soil dry weight and are expressed in units of nmol N gDW^{-1} d^{-1}

2.9. Statistical analyses

We sampled stem heights, stem density, and leaf density multiple times, and as a result, applied linear mixed-effects models for each parameter to determine differences between treatments. In this model framework, each experimental unit (tube) was used as a random intercept and number of days deployed was a continuous variable. We used mean live stem height per experimental unit. The models were checked for normality, and residuals versus fitted values were plotted and met assumptions. We used pairwise comparisons to determine differences between each treatment and days deployed combination (Table S4 in Supplement 2 at www.int-res.com/articles/suppl/m689p033_supp2.xlsx).

For parameters collected at the end of the experiment (biomass, gas fluxes, soil nutrients, and N cycling), we used linear regression to model each parameter as a function of mussel biomass. We focused on final mussel biomass, which was highly correlated with density, due to the spread and overlap in mussel biomass between treatments. We also used linear regression to model relationships between parameters (Table S2 in Supplement 1). Specifically, max gross CO_2 uptake was modeled as a function of mussel biomass and live leaf density. Because the trend was similar between these regressions, we conducted a linear regression of max gross CO_2 per leaf as a function of mussel biomass. Dark CO_2 flux (respiration) was modeled as a linear regression as a function of mussel biomass. Models were checked for normality, and residuals and fitted values were examined. No transformations were needed to meet model assumptions. We used the package 'lme4' for the linear mixed effect models and the 'lm' function in R for linear regressions (Bates et al. 2015, R Core Team 2018). An alpha of 0.05 was used to determine significance for all analyses.

3. RESULTS

3.1. Biomass and recruitment of *Geukensia granosissima* and other invertebrates

We observed *G. granosissima* recruits in every treatment, except treatment 1, at the end of the experiment, with treatment 4 having the most mussel recruits (Table S1). Recruitment resulted in treatment 0 having more *G. granosissima* than treatment 1 on average; however, *G. granosissima* in treatment 0 were smaller and were in 1 out of 4 replicates (Table 1; Table S1). A total of 3 mussels died by Day 11 of the experiment: 1 each from treatments 2, 4, and 8. In response, 3 mussels were replaced (Table S1). No mussels were lost (or replaced) after Day 11. In general, total *G. granosissima* biomass increased by the end of the experiment for all treatments (Table 1). Final *G. granosissima* biomass was significantly positively correlated to *G. granosissima* density (Pearson's correlation coefficient = 0.89; Table S3 in Supplement 1). Other invertebrates, such as *Littorina irrorata* and *Neritina usnea* were occasionally observed in the experimental units. Overall, 1 *L. irrorata* and 2 *N. usnea* were recorded over the course of the experiment (Table S1).

3.2. Impact of *G. granosissima* on plant growth

There was a positive linear increase in the number of live leaves across all treatments over the growing season (Fig. 1a). The interaction between treatment and days deployed was significant, which indicates differences in slopes between treatments over time (ANOVA of LME; MS = 23 381 455, $F_{4,315} = 20.03$, $p < 0.001$; Table 2). By the end of the experiment (Day 124), only live leaf density in treatment 8 was significantly different from treatment 0 (pairwise comparison; $t_{21.4} = -7.11$, $p < 0.001$; Table S4) with treatment 8 having 1.9 times more leaves than treatment 0 (Table 1). Similarly, the number of live stems across all treatments increased linearly over the growing season (Fig. 1b), and the interaction between treatment and days deployed was significant, which indicates differences in slopes between treatments over time (ANOVA of LME; MS = 1 747 819, $F_{4,315} = 25.73$, $p < 0.001$; Table 2). By the end of the experiment (Day 124), only stem density in treatment 8 was significantly different from treatment 0 (pairwise comparison; $t_{18.7} = -5.34$, $p = 0.02$; Table S4), with treatment 8 having 1.5 times more stems than treatment 0 (Table 1). Live stem height also increased over time,

Table 1. Means (±SD) for initial and final mussel density and biomass, final live leaf and stem density, height, above- and belowground biomass, gross CO_2 flux, dark CO_2 flux, maximum electron transport rate (ETR_{max}), final photosynthetic efficiency (α), CH_4 flux, nitrification potential, denitrification potential, NO_x, and NH_4

	Treatment				
	0	1	2	4	8
Mussels					
Initial density (m^{-2})	0	127	254	509	1018
Initial biomass (g m^{-2})	0	93 ± 51	150 ± 63	306 ± 107	485 ± 66
Final density (m^{-2})	64 ± 127	127 ± 0	350 ± 122	637 ± 275	1019 ± 104
Final biomass (g m^{-2})	3 ± 7	121 ± 37	233 ± 50	395 ± 186	626 ± 62
Plant growth					
Leaf density (m^{-2})	3978 ± 1041	5634 ± 1608	5156 ± 1304	5920 ± 1550	7734 ± 1082
Stem density (m^{-2})	2037 ± 681	2228 ± 482	1973 ± 760	2100 ± 482	3151 ± 700
Stem height (cm)	29 ± 25	38 ± 30	52 ± 45	50 ± 36	41 ± 31
Aboveground biomass (g m^{-2})	1302 ± 464	2067 ± 289	3556 ± 1176	3128 ± 662	3493 ± 426
Belowground biomass (g m^{-2})	372 ± 154	542 ± 296	755 ± 294	699 ± 242	1206 ± 439
CO_2 fluxes, photosynthesis, CH_4					
Gross CO_2 flux (mmol m^{-2} h^{-1})	−47 ± 12	−78 ± 35	−71 ± 24	−83 ± 12	−105 ± 25
Dark CO_2 flux (mmol m^{-2} h^{-1})	11 ± 5	20 ± 8	30 ± 11	33 ± 7	53 ± 9
ETR_{max} (µmol electrons m^{-2} s^{-1})	40 ± 16	62 ± 32	53 ± 14	48 ± 13	55 ± 17
α	0.11 ± 0.03	0.15 ± 0.05	0.13 ± 0.02	0.11 ± 0.04	0.13 ± 0.04
CH_4 flux (µmol m^{-2} h^{-1})	216 ± 117	264 ± 253	296 ± 142	303 ± 43	371 ± 82
Nitrogen cycling process rates and soil N					
Nitrification potential (nmol N gDW^{-1} d^{-1})	265 ± 46	619 ± 454	810 ± 605	963 ± 701	1491 ± 764
Denitrification potential (nmol N gDW^{-1} d^{-1})	1367 ± 648	2085 ± 866	1790 ± 441	1973 ± 730	2475 ± 263
NO_x (nmol N gDW^{-1})	3 ± 6	4 ± 3	3 ± 6	2 ± 2	9 ± 8
NH_4 (nmol N gDW^{-1})	343 ± 44	1145 ± 540	731 ± 366	1515 ± 1091	580 ± 216

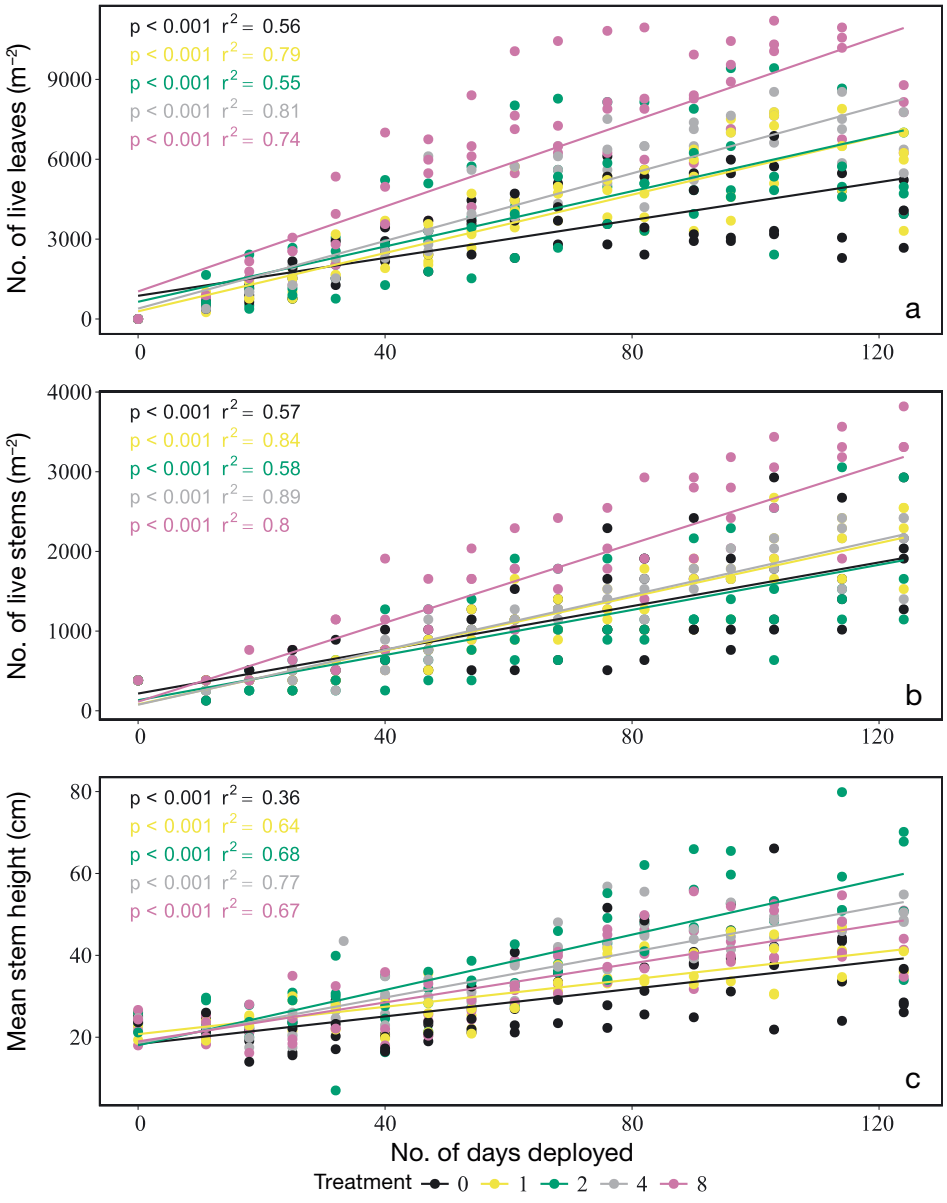

Fig. 1. Aboveground vegetation variables plotted against number of days deployed: (a) live leaves, (b) live stems, and (c) stem height. Colors correspond to mussel treatments as indicated in the key. p- and r^2-values are from each combination of treatment × days deployed (Table 2). Pairwise comparisons for each day sampled can be found in Table S4 in Supplement 2

and the interaction between treatment and days deployed was significant, which indicates a difference in slopes between treatments over time (ANOVA of LME; MS = 474.2, $F_{4,315}$ = 13.17, p < 0.001; Table 2). Stem height was only significantly different between treatment 0 and treatment 2 by the end of the experiment (pairwise comparison; $t_{30.48}$ = −6.35, p < 0.001; Table S4), with treatment 2 being 1.7 times taller than treatment 0 (Table 1). Aboveground biomass ranged from 853.1 g m^{-2} (treatment 0) to 4624.4 g m^{-2} (treatment 2) and increased by 3.35 g m^{-2} for each g m^{-2} of mussel biomass ($F_{1,18}$ = 20.84, r^2 = 0.53, p < 0.001; Tables 1 & 3). Live belowground biomass increased by 1.15 g m^{-2} for each g m^{-2} of mussel biomass ($F_{1,18}$ = 17.33, r^2 = 0.49, p < 0.001; Table 3), with a minimum of 172. 3 g m^{-2} in treatment 0 and a maximum of 1850.1 g m^{-2} in treatment 8 (Table 1).

3.3. Impact of *G. granosissima* on CO_2 fluxes, photosynthetic efficiency, and CH_4 fluxes

As mussel biomass increased, there was a linear decrease in maximum gross CO_2 uptake (linear regression; $F_{1,18}$ = 38.18, r^2 = 0.68, p < 0.01; Fig. 2a, Table 3) with maximum gross CO_2 uptake decreas-

Table 2. ANOVA table for the fixed effects of a model evaluating the impacts of mussel treatment and day deployed on vegetation characteristics (leaf density, stem density, stem height). These results indicate whether there are statistical differences in slope between each grouping of treatment × days deployed. See Table S4 in Supplement 2 for pairwise comparisons between each combination of treatment × days deployed. Treatment details are provided in Table 1

Model term	MS	df	*F*	p
Leaf density				
Treatment	368 508	4, 21	0.32	0.86
Days deployed	1 448 914 601	1, 315	1240.97	<0.001
Treatment:days deployed	23 381 455	4, 315	20.03	<0.001
Stem density				
Treatment	7757	4, 18	0.11	0.98
Days deployed	133 740 428	1, 315	1969.26	<0.001
Treatment:days deployed	1 747 819	4, 315	25.74	<0.001
Stem height				
Treatment	7.9	4, 29	0.22	0.93
Days deployed	25145.1	1, 315	698.26	<0.001
Treatment:days deployed	474.2	4, 315	13.17	<0.001

Regressions of each treatment × days deployed grouping

	R^2	df	*F*	p
Leaf density				
Treatment 0	0.55	1, 66	83.17	<0.001
Treatment 1	0.79	1, 66	254.8	<0.001
Treatment 2	0.55	1, 66	81.98	<0.001
Treatment 4	0.81	1, 66	284	<0.001
Treatment 8	0.74	1, 66	184.6	<0.001
Stem density				
Treatment 0	0.57	1, 66	88.5	<0.001
Treatment 1	0.84	1, 66	337.9	<0.001
Treatment 2	0.58	1, 66	90.86	<0.001
Treatment 4	0.89	1, 66	546.8	<0.001
Treatment 8	0.80	1, 66	265.8	<0.001
Stem height				
Treatment 0	0.36	1, 66	37.01	<0.001
Treatment 1	0.64	1, 66	115.9	<0.001
Treatment 2	0.68	1, 66	140.9	<0.001
Treatment 4	0.77	1, 66	226.9	<0.001
Treatment 8	0.67	1, 66	135.6	<0.001

ing by 0.53 mmol m^{-2} h^{-1} . These more negative fluxes indicate a higher rate of photosynthetic CO_2 uptake by the plants. There was also a negative linear relationship between maximum gross CO_2 uptake and live leaf density, with maximum gross CO_2 decreasing by 0.06 mmol m^{-2} h^{-1} for every m^2 of live leaves ($F_{1,18}$ = 18.75, r^2 = 0.51, p < 0.001; Fig. 2b, Table S2). When the maximum gross CO_2 flux was normalized to leaf density, the negative linear relationship between this CO_2 flux and mussel biomass remained, with maximum gross CO_2 per leaf decreasing by 0.006 mmol m^{-2} h^{-1} ($F_{1,18}$ = 13.79, r^2 = 0.43, p = 0.001; Fig. 2c, Table 3). There was a strong positive linear relationship between respiration (dark CO_2 flux) and mussel biomass ($F_{1,18}$ = 62.04, r^2 = 0.78, p < 0.001; Fig. 2d, Table 3), with a 0.06 mmol m^{-2} h^{-1} increase in respiration. The final photosynthetic capacity (ETR_{max}) ranged from 23.02 (treatment 0) to 107.4 (treatment 1) µmol electrons m^{-2} s^{-1} and had no trend with mussel biomass ($F_{1,18}$ = 1.62, r^2 = 0.08, p = 0.21; Tables 1 & 3). The final photosynthetic efficiency (α) ranged from 0.07 to 0.20 and had no trend with mussel biomass ($F_{1,18}$ = 0.12, r^2 = 0.00, p = 0.63; Tables 1 & 3). CH_4 flux was not significantly related to mussel biomass ($F_{1,18}$ = 2.12, r^2 = 0.10, p = 0.16; Tables 1 & 3, Fig. 3a). However, there was a positive linear increase in CH_4 flux as a function of increasing live root biomass, with CH_4 flux increasing 0.46 µmol m^{-2} h^{-1} ($F_{1,18}$ = 10.58, r^2 = 0.37, p = 0.004; Fig. 3b, Table S2).

Table 3. Linear regression results for final measures by final mussel biomass. Definitions as in Table 1

	Equation	R^2	df	*F*	p
Aboveground biomass	$y = 3.35x + 1784.93$	0.53	1, 18	20.84	<0.001
Belowground biomass	$y = 1.15x + 397.28$	0.49	1, 18	17.33	<0.001
Max. gross CO_2 per leaf	$y = -0.006x - 3.02$	0.43	1, 18	13.79	0.001
Max. gross CO_2	$y = -0.53x - 87.83$	0.68	1, 18	38.71	<0.001
Gross CO_2 flux	$y = -0.07x - 57.26$	0.36	1, 18	10.35	0.004
Dark CO_2 flux	$y = 0.06x + 13.20$	0.78	1, 18	62.04	<0.001
ETR_{max}	$y = -0.01x + 24.54$	0.08	1, 18	1.62	0.21
α	$y = 0.00x + 0.01$	0.00	1, 18	0.12	0.72
CH_4 flux	$y = 0.19x + 237.5$	0.10	1, 18	2.12	0.16
Nitrification potential	$y = 2.21x + 230$	0.59	1, 16	23.69	<0.001
Denitrification potential	$y = 1.49x + 1528.37$	0.27	1, 18	6.91	0.01
NO_x	$y = 0.005x + 3.05$	0.05	1, 18	1.09	0.30
NH_4	$y = 0.32x + 775.37$	0.01	1, 18	0.23	0.63

3.4. Impact of *G. granosissima* on nitrogen cycling process rates and soil nitrogen availability

Soil potential nitrification rates (linear regression; $F_{1,16}$ = 23.69, r^2 = 0.60, p < 0.01; Fig. 4a) and potential denitrification rates ($F_{1,18}$ = 6.91, r^2 = 0.28, p = 0.02; Fig. 4b) increased linearly by 2.21 (nitrification) and 1.49 (denitrification) nmol N gDW^{-1} d^{-1} with mussel biomass. Soil potential nitrification rates ranged from 212.3 (treatment 0) to 1491.8 (treatment 8) nmol N gDW^{-1} d^{-1}, and soil potential denitrification rates ranged from 505.4 (treatment 0)

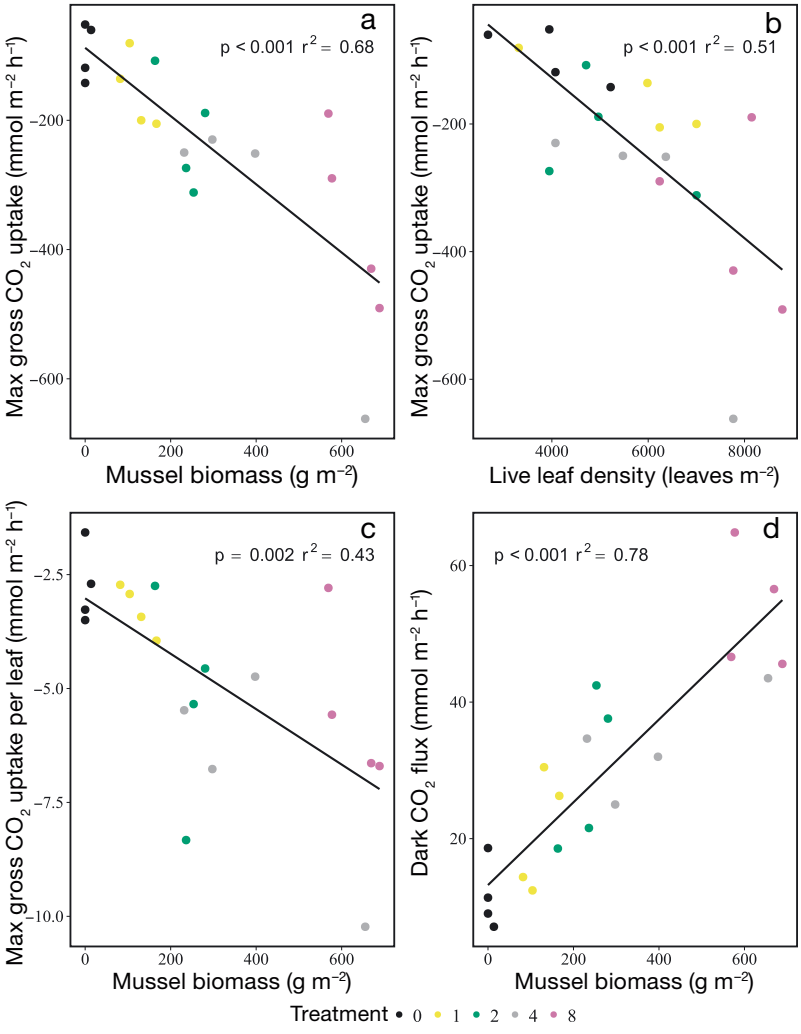

Fig. 2. Maximum gross CO_2 uptake plotted against (a) mussel biomass and (b) live leaf density; (c) maximum gross CO_2 uptake per leaf plotted against mussel biomass; and (d) dark CO_2 flux plotted against mussel biomass. Colors correspond to initial mussel treatments as indicated in the key. Lines represent linear regressions with corresponding r^2 on each graph

4. DISCUSSION

4.1. Impact of mussels on plant biomass

In eastern North American salt marshes, the presence of *Geukensia demissa* is associated with more and larger *Spartina alterniflora* (Bertness 1984, Angelini et al. 2016, Derksen-Hooijberg et al. 2018; Table S5 in Supplement 2). Stem height was also positively correlated with *G. demissa* biomass (Bertness 1984, Angelini et al. 2016; Table S5). We found similar responses in *S. alterniflora* biomass and size in response to *G. granosissima*. With *G. granosissima* presence (>127 mussels m^{-2}), we found taller stems and approximately 3 times greater aboveground biomass. We also found almost 3 times the amount of belowground biomass in the highest *G. granosissima* treatment compared to the zero *G. granosissima* treatment (even with some recruitment in the zero *G. granosissima* treatment). These results are consistent with observations from Sister Lake, LA, that found higher *G. granosissima* densities on shorelines with higher percent vegetation coverage and higher belowground biomass (Logarbo 2021; Table S5). These results differ with work in North Atlantic marshes that found no difference in stem density when *G. demissa* were planted with *S. alterniflora* (~300 mussels in a 0.25 m^{-2} quadrat), but these additions occurred on the marsh flat (>1 m from the edge) which may experience less stress and require less dense patches of *S. alterniflora* (Bertness 1984; Table S5).

to 3147.3 (treatment 1) nmol N gDW^{-1} d^{-1} (Tables 1 & 3). N cycling rates did not correlate with soil extractable nutrients (nitrification × NH_4; Pearson's correlation coefficient = −0.09; nitrification × NO_x; Pearson's correlation coefficient = −0.02; denitrification × NH_4; Pearson's correlation coefficient = 0.02; Denitrification × NO_x; Pearson's correlation coefficient = 0.14; Table S3 in Supplement 1). Soil potential rates had no trend with total live belowground plant biomass (nitrification: $F_{1,16} = 2.26$, $r^2 = 0.12$, $p = 0.15$; denitrification: $F_{1,18} = 0.69$, $r^2 = 0.03$, $p = 0.41$; Table S2). There was no significant trend between soil extractable ammonium content and mussel biomass ($F_{1,18} = 0.23$, $r^2 = 0.01$, $p = 0.63$; Table 3). There was also no detectable trend in soil extractable NO_x

4.2. Impact of mussels on plant productivity, respiration, and CH_4 fluxes

The larger and denser growth of *S. alterniflora* in the presence of *G. granosissima* drove an increase in CO_2 uptake by the plants. The maximum gross CO_2 uptake rates we measured, a proxy for gross primary productivity, became more negative (indicating more uptake) as a linear function of increasing *G. grano-*

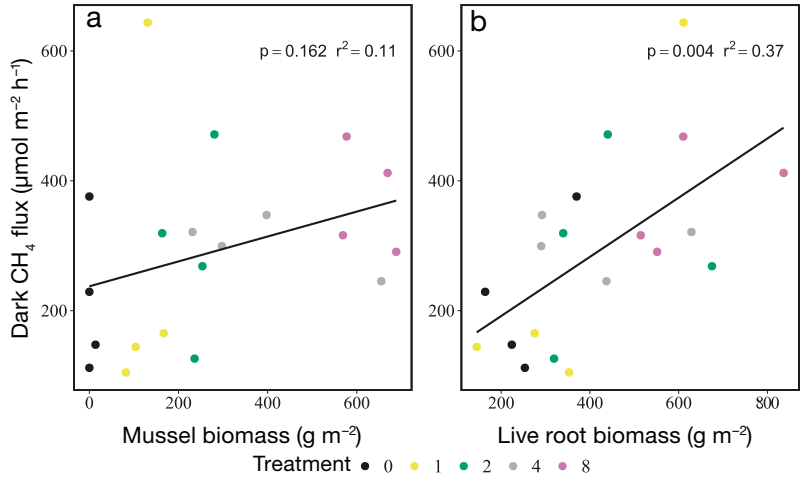

Fig. 3. CH_4 flux plotted against (a) mussel treatment and (b) live root biomass. Solid lines represent the mean flux for each treatment. Colors correspond to initial mussel treatments as indicated in the key. Lines represent linear regressions with corresponding r^2 on each graph

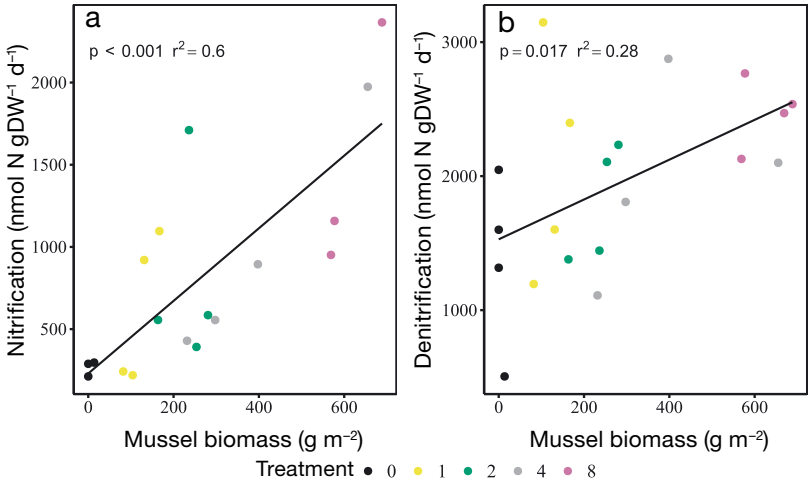

Fig. 4. Potential rates of (a) nitrification and (b) denitrification plotted against final mussel biomass. Colors correspond to initial mussel treatments as indicated in the key. Lines represent linear regressions with corresponding r^2 on each graph

sissima biomass. We suspect this is due to treatments with more *G. granosissima* having greater photosynthetic surface area through a combination of higher leaf densities and larger leaves. Though we did not measure leaf size, we can infer larger leaves through our observation that gross productivity per leaf increased as a function mussel biomass while photosynthetic efficiency (ETR_{max}) at the scale of individual leaves did not. Our results for CO_2 gross fluxes (–28 to –127 mmol CO_2 m^{-2} h^{-1} across all treatments) fall well outside of the range reported for an *S. alterniflora* salt marsh in Dauphin Island, AL (–8.6 to –36 mmol CO_2 m^{-2} h^{-1}) (Wilson et al. 2015). This difference may be due to the difference in mean salinity (20.7 vs. 6.9 in our study), the difference in study periods (February–June vs. June– October in our study), and differences in live aboveground biomass and or allometry (Wilson et al. 2015). Our CO_2 dark fluxes (respiration) were similar to the maximum respiration reported for *S. alterniflora* in Dauphin Island, AL, (28.1 mmol CO_2 m^{-2} h^{-1}) for treatments 2 and 4 (30.0 ± 11 and 33.7 ± 7 mmol CO_2 m^{-2} h^{-1}, respectively) and about 2 times greater for treatment 8 (53.4 ± 9 mmol CO_2 m^{-2} h^{-1}) (Ledford et al. 2020). Interestingly, the highest respiration (dark CO_2) fluxes reported by Ledford et al. (2020) came from plots in a high nutrient addition treatment with loading rates of 40 g N and 2.5 g P m^{-2} yr^{-1}.

Our CH_4 fluxes are similar to studies in our region (range of 0–252 µmol CH_4 m^{-2} h^{-1}, Wilson et al. 2015), and fall within the range of reported fluxes for salt marshes globally (–3 to 3922 µmol CH_4 m^{-2} h^{-1}, Al-Haj & Fulweiler 2020). In general, higher salinities drive lower CH_4 emissions from *S. alterniflora*-dominated salt marshes (Poffenbarger et al. 2011, Holmquist et al. 2018). Our study was conducted in a brackish marsh (salinity of water during gas flux sampling was 13.9), which could contribute to higher CH_4 emissions. Rietl et al. (2017) showed that CH_4 fluxes were higher from field enclosures with 12 *G. granosissima* m^{-2} than from enclosures with no *G. granosissima* during the warmest months of the year (July–October) when CH_4 fluxes were at their annual maximum. It is possible that *G. granosissima* stimulate microbial methanogenesis by injecting labile organic carbon in the soil and porewater through their metabolic activity (Bertness 1984, Bilkovic et al. 2017). Interestingly, we did not find a strong linear relationship between CH_4 fluxes and *G. granosissima* biomass, suggesting that the mechanism driving increased CH_4 fluxes may not be directly associated with the *G. granosissima* themselves. Rather, we found the CH_4 fluxes increased linearly with increasing root biomass (which in turn increased with increasing *G. granosissima* biomass). It is likely that at

least some of the observed increases in CH_4 emissions were due to increased CH_4 transport from the *S. alterniflora* roots, through its aerenchyma system, and into the atmosphere (Teal & Kanwisher 1966, Mendelssohn et al. 1981, Maricle & Lee 2002, 2007). However, it is also possible that roots facilitated CH_4 emissions by stimulating methanogenesis via root exudates (Cheng et al. 2007, Emery & Fulweiler 2014). Although we did not find a strong relationship between *G. granosissima* and CH_4 fluxes, the trend of increasing CH_4 flux with live root biomass is something that should be considered when planning blue carbon projects, as the emissions of CH_4 could offset benefits of C sequestration (Kroeger et al. 2017).

4.3. Impact of mussels on nitrogen cycling process rates and nitrogen removal

Mussels are important biodepositers and can provide a local source of nutrients for plant uptake and microbial processes (Bertness 1984, Angelini et al. 2016, Bilkovic et al. 2017, Derksen-Hooijberg et al. 2018). A mussel-driven increase in N availability is the most likely mechanism behind our observations of increased plant productivity and growth in the presence of mussels. Salt marsh primary production is often nitrogen limited (Tyler et al. 2003) and relief of this limitation may result in increased plant growth and productivity (Brewer 2003, Darby & Turner 2008, McFarlin et al. 2008, Ket et al. 2011, Davis et al. 2017) as well as respiration (Ledford et al. 2020).

G. demissa presence drove a doubling of porewater ammonia concentrations in South Atlantic *S. alterniflora* marshes (Angelini et al. 2016, Derksen-Hooijberg et al. 2018) most likely because about half of the nitrogen ingested by *Geukensia* species is excreted as ammonium with the rest used for growth, gametes, and byssal thread production (Jordan & Valiela 1982). We found that soil extractable ammonium was not significantly greater in the presence of *G. granosissima*, which could be due to salt marsh primary production generally being N limited and/or the fact that up to 95% of the NH_4^+ generated in soil can be taken up by salt marsh plants (Buresh et al. 1981, Smith & DeLaune 1985). It is possible that the majority of mussel-generated inorganic nitrogen in our experiment could have been rapidly taken up by the plants and fueled the observed plant growth. Soil extractable ammonium is also important in nitrification and could have contributed to our observation that potential nitrification rates increased as mussel biomass increased. This is consistent with previous work that found increases in nitrification when mussels and *S. alterniflora* co-occurred in Atlantic marshes (Bilkovic et al. 2017, Zhu et al. 2019). Increased potential nitrification is likely mediated either by mussels providing more nitrogen in surface sediments for microbes to metabolize, or via mussel feeding activity and bioturbation, which can oxidize the nitrogen-enriched surrounding soil (Bilkovic et al. 2017).

Denitrification is typically coupled with nitrification in salt marsh soils because nitrification generates the NO_x (nitrate or nitrite) substrate required by denitrifying microorganisms (Reddy et al. 1989, Thompson et al. 1995, Risgaard-Petersen & Jensen 1997, Dollhopf et al. 2005, Hopkinson & Giblin 2008). Therefore, higher nitrification rates likely drive an increase in denitrification rates by increasing the rate of NO_x supply. Our results align with similar work in Atlantic marshes that reported increased denitrification when *G. demissa* and *S. alterniflora* co-occurred (Bilkovic et al. 2017) and aligns with work demonstrating that other bivalves, such as oysters and clams, remove N through uptake of organic matter and enhancing denitrification rates in soil (Smyth et al. 2018). Our very low soil extractable NO_x concentrations likely result from a low rate of NOx supply from nitrification relative to the rate of NO_x removal by denitrification, consistent with these 2 nitrogen cycling processes being tightly coupled (Thompson et al. 1995, Dollhopf et al. 2005). Denitrification converts NO_x into inert N_2 gas and N_2O, making it an important removal pathway for bioavailable nitrogen in salt marsh soils. Our results, along with others, suggest that the positive relationship between *S. alterniflora* and mussels likely enhances N removal from salt marshes by promoting coupled denitrification–nitrification (Bilkovic et al. 2017, Zhu et al. 2019). The impact of this positive relationship on N removal is particularly important considering that 21% of coasts and 58% of rivers and streams in the USA have excess nutrients (US Environmental Protection Agency 2019) and because restoring or creating wetlands and living shorelines, including marshes, is one action that may be used to address nutrient-impaired waters (Land et al. 2016, Onorevole et al. 2018).

4.4. Conclusions

Our results support our hypothesis that increasing *G. granosissima* density would increase plant growth and biomass, gas exchange, and soil nitrogen-cycling process rates. Our study demonstrates that *G.*

granosissima shares a similar positive relationship with *S. alterniflora* as *G. demissa* does and supports previous work demonstrating the importance of this relationship for salt marsh ecosystem function and services. The observed positive relationships between *Geukensia* species biomass and *S. alterniflora* plant productivity, biomass, and vegetation characteristics (e.g. size and density) likely impact the production of ecosystem services in the marsh landscape, and as a result should be considered in the conservation and restoration of salt marsh landscapes (Bilkovic et al. 2021). For example, vegetation height and density impact sedimentation in the marsh landscape such that taller, denser *S. alterniflora* may capture more sediment (Christiansen et al. 2000, Mudd et al. 2010, Fagherazzi et al. 2012, Nardin et al. 2018). As a result, increased sediment capture may help marshes accrete and keep pace with sea level rise (Baustian et al. 2012). Similarly, increased sediment deposition may influence carbon accumulation in the marsh, depending on general sediment supply (Mudd et al. 2009). Additionally, denser stands of *S. alterniflora* better attenuate waves (Bouma et al. 2005, Ysebaert et al. 2011, Fagherazzi et al. 2012, Anderson & Smith 2014). Previous work has demonstrated that wave attenuation was 67% greater when *S. alterniflora* was planted with another bivalve, *Crassostrea virginica* (Manis et al. 2015). The positive relationship between mussel density and belowground biomass could have positive implications on marsh soil strength and erodibility, since several studies have demonstrated that belowground biomass is critical to maintain soil shear strength and minimize erodibility (Howes et al. 2010, Sasser et al. 2018, Gillen et al. 2021). This highlights the potential importance of positive species interactions in mediating ecosystem services like N removal, wave attenuation, sediment deposition, soil strength, and erosion in salt marshes.

Acknowledgements. We thank 3 anonymous reviewers and Megan La Peyre for comments that improved the manuscript. We thank Ekaterina Bulygina, Logan McPherson, Amanda Richey, and Stephanie Plaisance for field and laboratory assistance. This research was made possible by grants to B.J.R. from Louisiana Sea Grant (award GR-00003351) and from The Gulf of Mexico Research Initiative to the Coastal Waters Consortium. The funders had no role in the design, execution, or analyses of this project. This project was supported in part by R.E.R.'s appointment to the Research Participation Program at the Gulf Ecology Measurement and Modeling Division, US Environmental Protection Agency (EPA), administered by the Oak Ridge Institute for Science and Education through an interagency agreement between the US Department of Energy and the EPA.

LITERATURE CITED

Al-Haj AN, Fulweiler RW (2020) A synthesis of methane emissions from shallow vegetated coastal ecosystems. Glob Change Biol 26:2988–3005

Anderson ME, Smith J (2014) Wave attenuation by flexible, idealized salt marsh vegetation. Coast Eng 83:82–92

Angelini C, van der Heide T, Griffin JN, Morton JP and others (2015) Foundation species' overlap enhances biodiversity and multifunctionality from the patch to landscape scale in southeastern United States salt marshes. Proc R Soc B 282:20150421

Angelini C, Griffin JN, van de Koppel J, Lamers LP and others (2016) A keystone mutualism underpins resilience of a coastal ecosystem to drought. Nat Commun 7:12473

Bates D, Mächler M, Bolker B, Walker S (2015) Fitting linear mixed-effects models using lme4. J Stat Software 67:1–48

Baustian JJ, Mendelssohn IA, Hester MW (2012) Vegetation's importance in regulating surface elevation in a coastal salt marsh facing elevated rates of sea level rise. Glob Change Biol 18:3377–3382

Bernhard AE, Beltz J, Giblin AE, Roberts BJ (2021) Biogeography of ammonia oxidizers in New England and Gulf of Mexico salt marshes and the potential importance of comammox. ISME Commun 1:9

Bertness MD (1984) Ribbed mussels and *Spartina alterniflora* production in a New England salt marsh. Ecology 65:1794–1807

Bertness MD, Leonard GH (1997) The role of positive interactions in communities: lessons from intertidal habitats. Ecology 78:1976–1989

Bilkovic DM, Mitchell MM, Isdell RE, Schliep M, Smyth AR (2017) Mutualism between ribbed mussels and cordgrass enhances salt marsh nitrogen removal. Ecosphere 8: e01795

Bilkovic DM, Isdell RE, Guthrie AG, Mitchell MM, Chambers RM (2021) Ribbed mussel *Geukensia demissa* population response to living shoreline design and ecosystem development. Ecosphere 12:e03402

Bouma T, De Vries MB, Low E, Kusters L and others (2005) Flow hydrodynamics on a mudflat and in salt marsh vegetation: identifying general relationships for habitat characterisations. Hydrobiologia 540:259–274

Brewer JS (2003) Nitrogen addition does not reduce belowground competition in a salt marsh clonal plant community in Mississippi (USA). Plant Ecol 168:93–106

Bruno JF, Stachowicz JJ, Bertness MD (2003) Inclusion of facilitation into ecological theory. Trends Ecol Evol 18: 119–125

Buresh RJ, DeLaune RD, Patrick WH Jr (1981) Influence of *Spartina alterniflora* on nitrogen loss from marsh soil. Soil Sci Soc Am J 45:660–661

Cheng X, Peng R, Chen J, Luo Y and others (2007) CH_4 and N_2O emissions from *Spartina alterniflora* and *Phragmites australis* in experimental mesocosms. Chemosphere 68: 420–427

Chintala MM, Wigand C, Thursby G (2006) Comparison of *Geukensia demissa* populations in Rhode Island fringe salt marshes with varying nitrogen loads. Mar Ecol Prog Ser 320:101–108

Christiansen T, Wiberg P, Milligan T (2000) Flow and sediment transport on a tidal salt marsh surface. Estuar Coast Shelf Sci 50:315–331

Culhane FE, Frid CLJ, Royo Gelabert E, White L, Robinson LA (2018) Linking marine ecosystems with the services

they supply: What are the relevant service providing units? Ecol Appl 28:1740–1751
Darby FA, Turner RE (2008) Below- and aboveground biomass of *Spartina alterniflora*: response to nutrient addition in a Louisiana salt marsh. Estuar Coasts 31:326–334
Davis J, Currin C, Morris JT (2017) Impacts of fertilization and tidal inundation on elevation change in microtidal, low relief salt marshes. Estuar Coasts 40:1677–1687
Derksen-Hooijberg M, Angelini C, Lamers LPM, Borst A and others (2018) Mutualistic interactions amplify salt-marsh restoration success. J Appl Ecol 55:405–414
Dollhopf SL, Hyun JH, Smith AC, Adams HJ, O'Brien S, Kostka JE (2005) Quantification of ammonia-oxidizing bacteria and factors controlling nitrification in salt marsh sediments. Appl Environ Microbiol 71:240–246
Durand SE, Niespor R, Ador A, Govinda N, Candia M, Torres K (2020) Ribbed mussel in an urban waterway filters bacteria introduced by sewage. Mar Pollut Bull 161: 111629
Emery HE, Fulweiler RW (2014) *Spartina alterniflora* and invasive *Phragmites australis* stands have similar greenhouse gas emissions in a New England marsh. Aquat Bot 116:83–92
Fagherazzi S, Kirwan ML, Mudd SM, Guntenspergen GR and others (2012) Numerical models of salt marsh evolution: ecological, geomorphic, and climatic factors. Rev Geophys 50:RG1002
Gillen MN, Messerschmidt TC, Kirwan ML (2021) Biophysical controls of marsh soil shear strength along an estuarine salinity gradient. Earth Surf Dynam 9:413–421
Greenberg AE, Clesceri LS, Eaton AD (1992) Standard methods for the examination of water and wastewater. American Public Health Association, Washington, DC
Hill TD, Roberts BJ (2017) Effects of seasonality and environmental gradients on *Spartina alterniflora* allometry and primary production. Ecol Evol 7:9676–9688
Holmquist JR, Windham-Myers L, Bernal B, Byrd KB and others (2018) Uncertainty in United States coastal wetland greenhouse gas inventorying. Environ Res Lett 13: 115005
Honig A, Supan J, Peyre ML (2015) Population ecology of the gulf ribbed mussel across a salinity gradient: recruitment, growth and density. Ecosphere 6:226
Hopkinson CS, Giblin AE (2008) Nitrogen dynamics of coastal salt marshes. In: Capone DG, Bronk DA, Mulholland MR, Carpenter EJ (eds) Nitrogen in the marine environment, 2nd edn. Academic Press, San Diego, CA, p 991–1036
Howes NC, FitzGerald DM, Hughes ZJ, Georgiou IY and others (2010) Hurricane-induced failure of low salinity wetlands. Proc Natl Acad Sci USA 107:14014–14019
Jassby AD, Platt T (1976) Mathematical formulation of the relationship between photosynthesis and light for phytoplankton. Limnol Oceanogr 21:540–547
Jordan TE, Valiela I (1982) A nitrogen budget of the ribbed mussel, *Geukensia demissa*, and its significance in nitrogen flow in a New England salt marsh. Limnol Oceanogr 27:75–90
Ket WA, Schubauer-Berigan JP, Craft CB (2011) Effects of five years of nitrogen and phosphorus additions on a *Zizaniopsis miliacea* tidal freshwater marsh. Aquat Bot 95:17–23
Kreeger DA, Newell RIE (2001) Seasonal utilization of different seston carbon sources by the ribbed mussel, *Geukensia demissa* (Dillwyn) in a mid-Atlantic salt marsh. J Exp Mar Biol Ecol 260:71–91
Kreeger DA, Langdon CJ, Newell RIE (1988) Utilization of refractory cellulosic carbon derived from *Spartina alterniflora* by the ribbed mussel *Geukensia demissa*. Mar Ecol Prog Ser 42:171–179
Kroeger KD, Crooks S, Moseman-Valtierra S, Tang J (2017) Restoring tides to reduce methane emissions in impounded wetlands: a new and potent Blue Carbon climate change intervention. Sci Rep 7:11914
Land M, Granéli W, Grimvall A, Hoffmann CC, Mitsch WJ, Tonderski KS, Verhoeven JTA (2016) How effective are created or restored freshwater wetlands for nitrogen and phosphorus removal? A systematic review. Environ Evid 5:9
Ledford TC, Mortazavi B, Tatariw C, Mason OU (2020) Elevated nutrient inputs to marshes differentially impact carbon and nitrogen cycling in two northern Gulf of Mexico saltmarsh plants. Biogeochemistry 149:1–16
Logarbo J (2021) Incorporating life into living shorelines: Can Gulf ribbed mussels reduce shoreline erosion and enhance restoration practices? MSc thesis, Louisiana State University, Baton Rouge, LA
Manis JE, Garvis SK, Jachec SM, Walters LJ (2015) Wave attenuation experiments over living shorelines over time: a wave tank study to assess recreational boating pressures. J Coast Conserv 19:1–11
Maricle B, Lee R (2002) Aerenchyma development and oxygen transport in the estuarine cordgrasses *Spartina alterniflora* and *S. anglica*. Aquat Bot 74:109–120
Maricle B, Lee R (2007) Root respiration and oxygen flux in salt marsh grasses from different elevational zones. Mar Biol 151:413–423
Marton JM, Roberts BJ (2014) Spatial variability of phosphorus sorption dynamics in Louisiana salt marshes. J Geophys Res Biogeosci 119:451–465
Marton JM, Roberts BJ, Bernhard AE, Giblin AE (2015) Spatial and temporal variability of nitrification potential and ammonia-oxidizer abundances in Louisiana salt marshes. Estuar Coasts 38:1824–1837
McFarlin CR, Brewer JS, Buck TL, Pennings SC (2008) Impact of fertilization on a salt marsh food web in Georgia. Estuar Coasts 31:313–325
Mendelssohn IA, McKee KL, Patrick WH (1981) Oxygen deficiency in *Spartina alterniflora* roots: metabolic adaptation to anoxia. Science 214:439–441
Moody J, Kreeger D (2020) Ribbed mussel (*Geukensia demissa*) filtration services are driven by seasonal temperature and site-specific seston variability. J Exp Mar Biol Ecol 522:151237
Morris J (2007) Estimating net primary production of salt marsh macrophytes. In: Fahey TJ, Knapp AK (eds) Principles and standards for measuring primary production. Oxford University Press, p 106–119
Mudd SM, Howell SM, Morris JT (2009) Impact of dynamic feedbacks between sedimentation, sea-level rise, and biomass production on near-surface marsh stratigraphy and carbon accumulation. Estuar Coast Shelf Sci 82: 377–389
Mudd SM, D'Alpaos A, Morris JT (2010) How does vegetation affect sedimentation on tidal marshes? Investigating particle capture and hydrodynamic controls on biologically mediated sedimentation. J Geophys Res Earth Surf 115:F03029
Nardin W, Larsen L, Fagherazzi S, Wiberg P (2018) Tradeoffs among hydrodynamics, sediment fluxes and vegeta-

tion community in the Virginia Coast Reserve, USA. Estuar Coast Shelf Sci 210:98–108

Onorevole KM, Thompson SP, Piehler MF (2018) Living shorelines enhance nitrogen removal capacity over time. Ecol Eng 120:238–248

Platt T, Gallegos CL, Harrison WG (1980) Photoinhibition of photosynthesis in natural assemblages of marine phytoplankton. J Mar Res 38:687–701

Poffenbarger HJ, Needelman BA, Megonigal JP (2011) Salinity influence on methane emissions from tidal marshes. Wetlands 31:831–842

R Core Team (2018) R: a language and environment for statistical computing. R Foundation for Statistical Computing, Vienna

Ralph PJ, Gademann R (2005) Rapid light curves: a powerful tool to assess photosynthetic activity. Aquat Bot 82: 222–237

Reddy KR, Patrick WH Jr, Lindau CW (1989) Nitrification–denitrification at the plant root–sediment interface in wetlands. Limnol Oceanogr 34:1004–1013

Rietl AJ, Nyman JA, Lindau CW, Jackson CR (2017) Gulf ribbed mussels (*Geukensia granosissima*) increase methane emissions from a coastal *Spartina alterniflora* marsh. Estuar Coasts 40:832–841

Risgaard-Petersen N, Jensen K (1997) Nitrification and denitrification in the rhizosphere of the aquatic macrophyte *Lobelia dortmanna* L. Limnol Oceanogr 42:529–537

Sasser C, Evers-Hebert E, Holm G, Milan B, Sasser J, Peterson E, DeLaune R (2018) Relationships of marsh soil strength to belowground vegetation biomass in Louisiana coastal marshes. Wetlands 38:401–409

Schutte CA, Marton JM, Bernhard AE, Giblin AE, Roberts BJ (2020) No evidence for long-term impacts of oil spill contamination on salt marsh soil nitrogen cycling processes. Estuar Coasts 43:865–879

Smith CJ, DeLaune RD (1985) Recovery of added ^{15}N-labelled ammonium-N from Louisiana Gulf Coast estuarine sediment. Estuar Coast Shelf Sci 21:225–233

Smyth AR, Murphy AE, Anderson IC, Song B (2018) Differential effects of bivalves on sediment nitrogen cycling in a shallow coastal bay. Estuar Coasts 41:1147–1163

Sørensen J (1978) Denitrification rates in a marine sediment as measured by the acetylene inhibition technique. Appl Environ Microbiol 36:139–143

Spicer J (2007) A comparison of channel morphology, marsh elevation and biological processes in natural and dredged tidal salt marshes in Louisiana. Dissertation, Louisiana State University, Baton Rouge, LA

Stachowicz JJ (2001) Mutualism, facilitation, and the structure of ecological communities: Positive interactions play a critical, but underappreciated, role in ecological communities by reducing physical or biotic stresses in existing habitats and by creating new habitats on which many species depend. Bioscience 51:235–246

Teal JM, Kanwisher JW (1966) Gas transport in the marsh grass, *Spartina alterniflora*. J Exp Bot 17:355–361

Thompson SP, Paerl HW, Go MC (1995) Seasonal patterns of nitrification and denitrification in a natural and a restored salt marsh. Estuaries 18:399–408

Tyler AC, Mastronicola TA, McGlathery KJ (2003) Nitrogen fixation and nitrogen limitation of primary production along a natural marsh chronosequence. Oecologia 136: 431–438

US Environmental Protection Agency (2019) How's my waterway? https://mywaterway.epa.gov/ (accessed 7 December 2021)

Vastano A, Able K, Jensen O, Lopez C, Martin C, Roberts B (2017) Age validation and seasonal growth patterns of a subtropical marsh fish: the Gulf killifish, *Fundulus grandis*. Environ Biol Fishes 100:1315–1327

Wilson BJ, Mortazavi B, Kiene RP (2015) Spatial and temporal variability in carbon dioxide and methane exchange at three coastal marshes along a salinity gradient in a northern Gulf of Mexico estuary. Biogeochemistry 123:329–347

Ysebaert T, Yang SL, Zhang L, He Q, Bouma TJ, Herman PMJ (2011) Wave attenuation by two contrasting ecosystem engineering salt marsh macrophytes in the intertidal pioneer zone. Wetlands 31:1043–1054

Zhu J, Zarnoch C, Gosnell JS, Alldred M, Hoellein T (2019) Ribbed mussels *Geukensia demissa* enhance nitrogen-removal services but not plant growth in restored eutrophic salt marshes. Mar Ecol Prog Ser 631:67–80

Editorial responsibility: Jana Davis, Annapolis, Maryland, USA
Reviewed by: D. Liu and 2 anonymous referees

Submitted: August 25, 2021
Accepted: March 9, 2022
Proofs received from author(s): May 8, 2022